Distributed MIMO Networks with Rotary ULAs for Indoor Scenarios under Rician Fading

(article starts on next page)

Distributed MIMO Networks With Rotary ULAs for Indoor Scenarios Under Rician Fading

EDUARDO N. TOMINAGA [1] (Graduate Student Member, IEEE),
ONEL L. A. LÓPEZ [1] (Senior Member, IEEE), TOMMY SVENSSON [2] (Senior Member, IEEE),
RICHARD D. SOUZA [3] (Senior Member, IEEE), AND HIRLEY ALVES [1] (Member, IEEE)

[1]Centre for Wireless Communications, University of Oulu, 90570 Oulu, Finland

[2]Communication Systems Group, Chalmers University of Technology, 412 96 Gothenburg, Sweden

[3]Department of Electrical and Electronics Engineering, Federal University of Santa Catarina, Florianópolis 88040-370, Brazil

CORRESPONDING AUTHOR: E. N. TOMINAGA (e-mail: eduardo.noborotominaga@oulu.fi)

ABSTRACT The Fifth-Generation (5G) wireless communications networks introduced native support for Machine-Type Communications (MTC) use cases. Nevertheless, current 5G networks cannot fully meet the very stringent requirements regarding latency, reliability, and number of connected devices of most MTC use cases. Industry and academia have been working on the evolution from 5G to Sixth Generation (6G) networks. One of the main novelties is adopting Distributed Multiple-Input Multiple-Output (D-MIMO) networks. However, most works studying D-MIMO consider antenna arrays with no movement capabilities, even though some recent works have shown that this could bring substantial performance improvements. In this work, we propose the utilization of Access Points (APs) equipped with Rotary Uniform Linear Arrays (RULAs) for this purpose. Considering a spatially correlated Rician fading model, the optimal angular position of the RULAs is jointly computed by the central processing unit using particle swarm optimization as a function of the location of the active devices. Considering the impact of imperfect location estimates, our numerical results show that the RULAs's optimal rotation brings substantial performance gains in terms of mean per-user spectral efficiency. The improvement grows with the strength of the line-of-sight components of the channel vectors. Given the total number of antenna elements, we study the trade-off between the number of APs and the number of antenna elements per AP, revealing an optimal number of APs for the cases of APs equipped with static ULAs and RULAs.

INDEX TERMS 6G, distributed MIMO, location-based beamforming, machine-type communications, particle swarm optimization.

I. INTRODUCTION

THE FIFTH Generation (5G) of wireless communication networks is currently under deployment and in advanced phases of standardization worldwide. Besides offering enhanced coverage capabilities and data rates for human-type communication applications such as mobile broadband Internet connectivity, which corresponds to a natural evolution of previous generations, 5G also offers services for a variety of Machine-Type Communication (MTC) applications [1]. 5G MTC use cases are traditionally split into two broad categories: massive MTC (mMTC) and Ultra-Reliable Low Latency Communications (URLLC), also known as critical MTC (cMTC). The former aims to provide wireless connectivity to a massive number of low-power and low-complexity devices in applications with moderate data rates, latency, and reliability requirements. The latter

category comprises applications with very stringent requirements in terms of latency and reliability. For instance, in an industrial setting, mMTC would correspond to sensors and actuators monitoring and controlling non-critical processes. In contrast, cMTC connectivity would enable critical control and safety systems to operate wirelessly [2].

The requirements of the different mMTC and cMTC use cases are foreseen to become even more stringent in future Sixth Generation (6G) networks. Thus, academia and industry have joined efforts in enhancing current technologies and developing new ones [3]. One of the novelties that have mostly attracted the attention of academia and industry is Distributed Multiple-Input Multiple Output (D-MIMO), often referred to as Cell-Free massive MIMO [4], [5], [6]. Instead of having a single base station equipped with several antenna elements serving a coverage area, the antenna elements are distributed among multiple Access Points (APs) over the coverage area. The APs are connected to a common Central Processing Unit (CPU) through fronthaul links. Such an approach provides a more uniform wireless coverage, enhancing network performance.

The vast majority of works investigating the performance of D-MIMO networks consider fixed antenna arrays, i.e., antenna arrays with no movement capabilities. Nevertheless, the idea of antenna arrays that can move has gained attention among the research community [7], [8], [9], [10], [11], [12], [13]. According to recent works [12], [13], [14], moving and/or rotating antennas can take advantage of spatially varying channel conditions within a confined area. Indeed, by altering the position and/or orientation of the antenna, better channel conditions can be achieved. In MTC scenarios, devices are typically deployed in fixed locations, while the surrounding environment may change over time, leading to slowly varying wireless channels. In use cases without mobility, narrowband MTC offers limited time and frequency diversity, which restricts the potential for improving data rates and transmission reliability. In such situations, antennas with movement capabilities are a promising solution for achieving higher spatial diversity gains. The related works will be discussed in more detail in the following subsection.

A. RELATED WORKS

The utilization of antenna arrays with movement capabilities is not new. For instance, the authors in [15] proposed a Direction of Arrival (DOA) estimation method that utilizes a Rotary Uniform Linear Array (RULA) and achieves satisfactory performance for under-determined DOA estimations, where the number of source signals can be larger than the number of receive antenna elements. The achievable rate performance of point-to-point Line-of-Sight (LoS) links with both the transmitter and receiver equipped with a RULA was studied in [7] and shown to approach the LoS capacity at any desired Signal-to-Noise Ratio (SNR). López et al. [8], [9] and Lin et al. [10] proposed the utilization of RULAs for wireless energy transfer. They studied a system where a power beacon equipped with a

RULA constantly rotates and transmits energy signals in the downlink to several low-power devices. The devices harvest energy from the transmitted signal to recharge their batteries. The authors in [11] developed and tested a prototype for hybrid mechanical-electrical beamforming for mmWave WiFi. Their experimental results in a point-to-point setup showed that the optimal rotation of the antenna array can bring significant throughput improvements for both LoS and Non-LoS (NLoS) scenarios.

More recently, movable antennas, which can move along one or several directions within a confined area, have been proposed [12], [13]. The main drawback of their utilization is that each movable antenna requires at least two cables and two servo motors, representing high deployment, operation, and maintenance costs. A different case is that of UAVs operating as flying base stations [16], which can also be interpreted as APs with movement capabilities. Their most notable advantage is that they present several degrees of freedom for movement since a UAV can be positioned at any point of the coverage area, at any height, and their position can be easily changed. However, their main drawbacks are limited carrying capacity, very high power consumption, and the consequent need for frequent recharges [17].

To the best of the authors' knowledge, this paper is the first work that investigates a D-MIMO network implemented with APs equipped with RULAs.[1] The most important advantages of the RULAs, when compared to the alternative approaches, are the lower deployment, operation, and maintenance costs since each AP requires a single servo-motor to rotate its Uniform Linear Array (ULA).

B. CONTRIBUTIONS AND ORGANIZATION OF THE PAPER

In this work, we evaluate the performance of D-MIMO networks for indoor industrial networks. We consider the uplink of a fully centralized system, where all APs simultaneously serve all the active Machine-Type Devices (MTDs). All APs are equipped with static ULAs or RULAs and connected to a common CPU through fronthaul links. The contributions of this work are listed below:

- We propose a scheme for joint configuration of the angular positions of all the RULAs in the system to maximize the mean per-user achievable Spectral Efficiency (SE). We assume that the network obtains estimates of the locations of the active devices (i.e., the devices that seek to transmit data in the uplink) before the data transmission phase and using some indoor localization method. The estimates are utilized to compute the optimal angular positions of the RULAs of the APs using the Particle Swarm Optimization (PSO).

---

[1]Preliminary results of this work were published in the conference version [18]. In that work, we consider a similar scenario but only a single AP. Since the optimization problem studied in that work has only one variable (we optimize the angular position of only a single AP), brute force search was used instead of PSO.

TABLE 1. List of acronyms.

Acronym	Definition
AP	Access Point
CPU	Central Processing Unit
CSI	Channel State Information
D-MIMO	Distributed MIMO
LoS	Line-of-Sight
MIMO	Multiple-Input Multiple-Output
MTD	Machine-Type Device
NLoS	Non-LoS
PSO	Particle Swarm Optimization
RA	Random Access
RULA	Rotary ULA
SE	Spectral Efficiency
SNR	Signal-to-Noise Ratio
SINR	Signal-to-Interference-plus-Noise Ratio
ULA	Uniform Linear Array
ZF	Zero Forcing

FIGURE 1. Illustration of the considered system model for $l = 50$ m, $Q = 4$, and $K = 16$.

- Adopting a spatially correlated Rician fading channel model, we evaluate the performance of the different setups considering different values of the Rician factor. Our numerical results show that the optimal rotation of the RULAs can substantially improve the mean-per-user achievable SE and that the performance gains grow with the strength of the LoS components of the channel vectors.
- We propose a localization error model and define different levels of localization accuracy based on the requirements specified by the Third Generation Partnership Project (3GPP) standards. The system's performance is evaluated as a function of the localization accuracy. Our numerical results show that the optimal rotation of the RULAs brings performance gains even when the system's localization accuracy is poor.
- We evaluate the trade-off between the number of APs and antennas per AP given a total number of antenna elements. Our numerical results show that for both the cases of APs equipped with static ULAs and APs equipped with RULAs, there is an optimal number of APs that achieves the highest SE values.

Table 1 lists the acronyms used throughout this paper alphabetically. This paper is organized as follows. Section II presents the system model. Section III introduces the localization error model. Section IV describes the proposed mechanism for optimizing the angular position of the RULAs. Section V presents and discusses the numerical results. Finally, Section VI concludes the paper.

Notation: lowercase boldface letters denote column vectors, while boldface uppercase letters denote matrices. a_i is the i-th element of the column vector $\mathbf{a}$, while $\mathbf{a}_i$ is the i-th column of the matrix $\mathbf{A}$. $\mathbf{I}_M$ is the identity matrix with size $M \times M$. The superscripts $(\cdot)^T$ and $(\cdot)^H$ denote the transpose and the conjugate transpose of a vector or matrix,
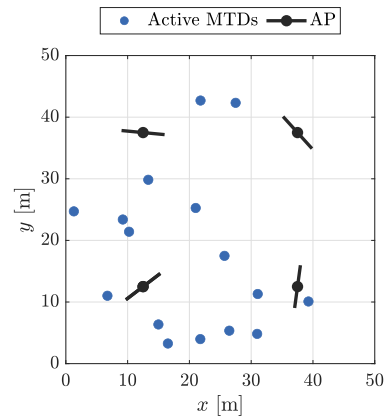
respectively. The scalar quantity's magnitude or the set's cardinality is denoted by $|\cdot|$, and $\|\cdot\|$ denotes the Euclidian norm of a vector (2-norm). We denote the one-dimensional uniform distribution with bounds a and b by $\mathcal{U}(a, b)$. We denote the multivariate Gaussian distribution with mean $\mathbf{a}$ and covariance $\mathbf{B}$ by $\mathcal{N}(\mathbf{a}, \mathbf{B})$.

II. SYSTEM MODEL

Similar to simulation setups of many relevant and related works (see, for instance, [4], [19], [20], [21]), we consider a square coverage area with dimensions $l \times l$ m². Q APs serve the coverage area, each with a RULA of S half-wavelength spaced antenna elements. The APs are at height h_{AP}. The Q APs jointly serve K MTDs that are active simultaneously and transmit data in the uplink. The locations of the MTDs are fixed, that is, we consider a scenario with no mobility. Let (x_k, y_k) denote the coordinates of the k-th MTD. For simplicity, we consider that the antenna elements of all MTDs are located at the same height h_{MTD} [4], [5]. The system model is illustrated in Fig. 1.

We consider fully centralized[2] processing: all the APs are connected to a common CPU through high-capacity fronthaul connections. The CPU is responsible for performing the following signal-processing tasks:

1) MTD's activity detection and identification.
2) Computation of the estimates of the locations of the active MTDs using an indoor localization method.
3) Computation of the optimal angular positions of the RULAs based on the estimated locations of the active MTDs.
4) Scheduling of the uplink data transmissions.

---

[2]In this work, for the sake of simplicity and to highlight the novelty of our proposed framework, we assume that all APs are perfectly calibrated and synchronized, a common assumption in several relevant works (e.g., [4], [19], [20], [21]). Note that imperfect synchronization can affect any D-MIMO system in both cases of APs equipped with static or rotary/movable antennas. Nevertheless, there is no indication that any alternatives would be more or less sensitive to synchronization.

5) Computation of the Channel State Information (CSI) of the links between any AP and any MTD using pilot sequences.
6) Computation of centralized receive combining vectors based on the global CSI knowledge.
7) Linear centralized uplink data decoding.

Further details on each of these tasks are provided in the subsequent sections of this work.

A. CHANNEL MODEL

We adopt a spatially correlated Rician fading channel model [22]. Let $\mathbf{h}_{kq} \in \mathbb{C}^{S \times 1}$ denote channel vector between the k-th MTD and the q-th AP, which can be modeled as [23]

$$\mathbf{h}_{kq} = \sqrt{\frac{\kappa}{1+\kappa}} \mathbf{h}_{kq}^{\text{los}} + \sqrt{\frac{1}{1+\kappa}} \mathbf{h}_{kq}^{\text{nlos}}, \qquad (1)$$

where κ is the Rician factor, $\mathbf{h}_{kq}^{\text{los}} \in \mathbb{C}^{S \times 1}$ is the deterministic LoS component, and $\mathbf{h}_{kq}^{\text{nlos}} \in \mathbb{C}^{S \times 1}$ is the random NLoS component.

The deterministic LoS component is given by

$$\mathbf{h}_{kq}^{\text{los}} = \sqrt{\beta_{kq}} \begin{bmatrix} 1 \\ \exp(-j2\pi \Delta \sin(\phi_{kq})) \\ \exp(-j4\pi \Delta \sin(\phi_{kq})) \\ \vdots \\ \exp(-j2\pi (S-1) \Delta \sin(\phi_{kq})) \end{bmatrix}, \qquad (2)$$

where β_{kq} is the power attenuation owing to the distance between the k-th MTD and the q-th AP, and $\phi_{kq} \in [0, 2\pi]$ is the azimuth angle relative to the boresight of the ULA of the q-th AP. Meanwhile, the random NLoS component is distributed as

$$\mathbf{h}_{kq}^{\text{nlos}} \sim \mathcal{CN}(\mathbf{0}, \mathbf{R}_{kq}). \qquad (3)$$

Note that

$$\mathbf{h}_{kq} \sim \mathcal{CN}\left(\sqrt{\frac{\kappa}{1+\kappa}} \mathbf{h}_{kq}^{\text{los}}, \frac{\mathbf{R}_{kq}}{\kappa+1}\right), \qquad (4)$$

where $\mathbf{R}_{kq} \in \mathbb{C}^{M \times M}$ is the positive semi-definite covariance matrix describing the spatial correlation of the NLoS components.

The spatial covariance matrices can be (approximately) modeled using the Gaussian local scattering model [24, Sec. 2.6]. Specifically, the s-th row, m-th column element of the correlation matrix is

$$[\mathbf{R}_{kq}]_{s,m} = \frac{\beta_{kq}}{N} \sum_{n=1}^{N} \exp[j\pi(s-m)\sin(\psi_{kq,n})]$$
$$\times \exp\left\{-\frac{\sigma_\phi^2}{2}[\pi(s-m)\cos(\psi_{kq,n})]^2\right\}, \quad (5)$$

where N is the number of scattering clusters, $\psi_{kq,n}$ is the nominal angle of arrival for the n-th cluster, and σ_ψ is the angular standard deviation.

B. SIGNAL MODEL

Herein, we consider an uplink scenario where K active MTDs simultaneously transmit signals to the Q APs. Let $M = QS$ denote the total number of receive antenna elements. The collective vector of wireless channel coefficients between the k-th MTD and the Q APs is $\mathbf{h}_k = [\mathbf{h}_{k1}^T, \mathbf{h}_{k2}^T, \ldots, \mathbf{h}_{kQ}^T]^T \in \mathbb{C}^{M \times 1}$.

The matrix $\mathbf{H} \in \mathbb{C}^{M \times K}$ containing the channel vectors of the K MTDs can be written as

$$\mathbf{H} = [\mathbf{h}_1, \mathbf{h}_2, \ldots, \mathbf{h}_K]. \qquad (6)$$

The $M \times 1$ collective received signal vector can be written as

$$\mathbf{y} = \sqrt{p}\mathbf{H}\mathbf{x} + \mathbf{n}, \qquad (7)$$

where p is the fixed uplink transmit power that is the same for all MTDs, $\mathbf{x} \in \mathbb{C}^{K \times 1}$ is the vector of symbols simultaneously transmitted by the K MTDs, and $\mathbf{n} \in \mathbb{C}^{M \times 1}$ is the vector of additive white Gaussian noise samples such that $\mathbf{n} \sim \mathcal{CN}(\mathbf{0}_{M \times 1}, \sigma_n^2 \mathbf{I}_M)$.

Let $\mathbf{V} \in \mathbb{C}^{M \times K}$ be a linear detector matrix used for the joint decoding of the signals transmitted from the K MTDs at all the APs. The received signal after the linear detection operation is split in K streams and given by

$$\mathbf{r} = \mathbf{V}^H \mathbf{y} = \sqrt{p}\mathbf{V}^H \mathbf{H}\mathbf{x} + \mathbf{V}^H \mathbf{n}. \qquad (8)$$

Let r_k and x_k denote the k-th elements of $\mathbf{r}$ and $\mathbf{x}$, respectively. Then, the received signal corresponding to the k-th MTD is

$$r_k = \underbrace{\sqrt{p}\mathbf{v}_k^H \mathbf{h}_k x_k}_{\text{Desired signal}} + \underbrace{\sqrt{p}\mathbf{v}_k^H \sum_{k' \neq k}^{K} \mathbf{h}_{k'} x_{k'}}_{\text{Inter-user interference}} + \underbrace{\mathbf{v}_k^H \mathbf{n}}_{\text{Noise}}, \qquad (9)$$

where $\mathbf{v}_k$ and $\mathbf{h}_k$ are the k-th columns of the matrices $\mathbf{V}$ and $\mathbf{H}$, respectively.

From (9), the Signal-to-Interference-plus-Noise Ratio (SINR) of the uplink transmission from the k-th MTD to all the APs is given by

$$\gamma_k = \frac{p|\mathbf{v}_k^H \mathbf{h}_k|^2}{p \sum_{k' \neq k}^{K} |\mathbf{v}_k^H \mathbf{h}_{k'}|^2 + \sigma_n^2 \|\mathbf{v}_k^H\|^2}. \qquad (10)$$

The receive combining matrix $\mathbf{V}$ is computed as a function of the matrix of estimated channel vectors $\hat{\mathbf{H}} \in \mathbb{C}^{M \times K}$, $\hat{\mathbf{H}} = [\hat{\mathbf{h}}_1, \ldots, \hat{\mathbf{h}}_K]$. In this work, we adopt the centralized Zero Forcing (ZF) combining scheme.[3] The receive combining matrix is computed as [27]

$$\mathbf{V} = \hat{\mathbf{H}}\left(\hat{\mathbf{H}}^H \hat{\mathbf{H}}\right)^{-1}. \qquad (11)$$

---

[3]Centralized ZF for distributed massive MIMO in indoor industrial scenarios was also adopted in [25]. Note that the performance obtained with ZF approaches that with MMSE in the high SINR regime [26], with the advantage of not requiring statistical knowledge of the noise variance or interference.

C. PERFORMANCE METRICS

To illustrate the improvement in the deterministic LoS links owing to the optimal rotations of the RULAs, we adopt the mean per-user achievable SE as the performance metric. The achievable uplink SE of the k-th MTD is

$$R_k = \mathbb{E}_\mathbf{H}\{\log_2(1 + \gamma_k)\}. \tag{12}$$

Then, the mean per-user achievable uplink SE is obtained by averaging over the achievable uplink SE of all the K active MTDs, i.e.,

$$\bar{R} = \frac{1}{K}\sum_{k=1}^{K} R_k. \tag{13}$$

D. IMPERFECT CSI MODEL

Assuming τ_p orthogonal pilot sequences during the uplink data transmission phase, such that $\tau_p \geq K$, and least squares channel estimation, the true channel realizations and the channel estimation errors are uncorrelated [28]. Then, the estimated channel vector of the k-th MTD, $\hat{\mathbf{h}}_k \in \mathbb{C}^{M \times 1}$, can be modeled as the sum of the true channel vector plus a random error vector as [28], [29], [30]

$$\hat{\mathbf{h}}_k = \mathbf{h}_k + \tilde{\mathbf{h}}_k, \tag{14}$$

where $\tilde{\mathbf{h}}_k \sim \mathcal{CN}(\mathbf{0}, \sigma_{\text{csi}}^2 \mathbf{I}_M)$ is the vector of channel estimation errors.

The parameter σ_{csi}^2 indicates the quality of the channel estimates. Let $\rho = p/\sigma_n^2$ denote the transmit SNR. We also assume that the duration of the uplink pilot transmission phase is equal to τ_p symbols. Then, the variance of the channel estimation errors can be modeled as a decreasing function of ρ as [28], [29], [30]

$$\sigma_{\text{csi}}^2 = \frac{1}{\tau_p \rho}. \tag{15}$$

Note that the channel estimation error depends only on the uplink transmit power, average receive noise power and number of orthogonal pilots, thus it is the same for all devices. The consequence of imperfect CSI is a slight decrease in the mean per-user achievable SEs compared to the case of perfect CSI for both the cases of static ULAs and RULAs.

E. PROPOSED FRAMEWORK

In this subsection, we describe our proposed framework for the optimization of the rotation of the Q APs and subsequent uplink data transmission. We assume that the same subset of devices is active during a period of time that spans multiple consecutive time slots. For instance, the devices could be video surveillance cameras [31] or smart utility meters [32]. Therefore, we assume that the optimization of the angular positions of the RULAs is performed before the data transmission phase, thus the angular positions of the RULAs is kept constant during multiple consecutive time slots. Inspired by the three-phase scheduled random access scheme from [33], our framework has the following phases:

1) Active MTDs, i.e., MTDs seeking to send data to the network, transmit non-orthogonal uplink pilots for activity detection.
2) The network identifies the set of active MTDs and, utilizing some indoor localization techniques [34], [35], [36], obtains estimates of the locations of the active MTDs.
3) The network assumes pure LoS propagation and utilizes the estimated locations of the MTDs and location-based beamforming to compute its optimal rotation and/or position. The RULAs have their angular positions updated accordingly.
4) The network broadcasts a common downlink feedback message to assign each device an orthogonal pilot sequence.
5) The MTDs transmit their orthogonal pilot sequences and data during multiple time slots. The uplink orthogonal pilots are used to compute the CSI estimates shown in (14) for each coherence time interval, which are then used to compute the ZF receive combining vectors in (11).

The proposed framework is illustrated in Fig. 2. Note that phase 5 extends over T time slots. Within each time slot, the K active devices transmit simultaneously. Each time slot is as long as the channel's coherence time interval and contains τ_c symbols. The first τ_p symbols of each time slot are used for the transmission of the orthogonal pilot sequences, while the remaining $\tau_d = \tau_c - \tau_p$ symbols are utilized for uplink data transmission. The numerical results presented in this work, that is, the mean per-user achievable SE presented in Section II-C, correspond to the performance achieved during phase 5.

III. LOCALIZATION ERROR MODEL

As mentioned in Section II-E, the CPU utilizes the information about the locations of the MTDs to compute the optimal rotations of the RULAs. However, the estimates of the locations are not perfect in practical systems. In this section, we propose a mathematical model for the localization error and relate it to the localization accuracy requirements proposed by 3GPP.

Considering that all the MTDs are located at the same height h_{MTD}, the imperfect localization impairment refers to the uncertainty on the location of the MTDs only on the horizontal plane. Let $\mathbf{p}_k = (x_k, y_k)$ denote the true location of the k-th MTD, and $\hat{\mathbf{p}}_k = (\hat{x}_k, \hat{y}_k)$ denote the estimated location. The localization error vector associated to the k-th MTD becomes

$$\mathbf{e}_k = \mathbf{p}_k - \hat{\mathbf{p}}_k = (x_{e,k}, y_{e,k}), \tag{16}$$

where $x_{e,k} = x_k - \hat{x}_k$ and $y_{e,k} = y_k - \hat{y}_k$ are the x and y components of the localization error vector, respectively. We can rewrite the localization error vector in polar form as

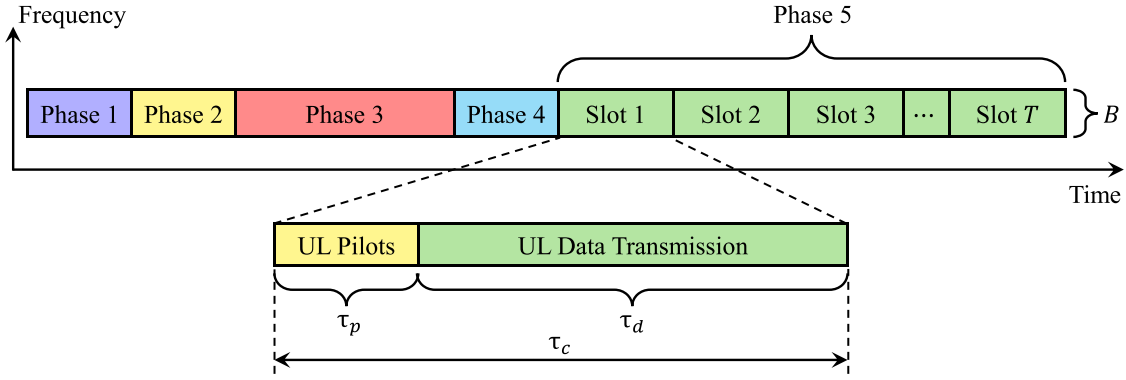$$\mathbf{e}_k = r_{e,k} \angle \theta_{e,k}, \tag{17}$$

FIGURE 2. Illustration of the proposed framework for the optimization of the angular positions of the RULAs and uplink data transmission. Note that the phases have different duration.

where $r_{e,k} = \sqrt{x_{e,k}^2 + y_{e,k}^2}$ and $\theta_{e,k} = \tan^{-1}(y_{e,k}/x_{e,k})$ are the magnitude and phase of the localization error vector, respectively.

Aiming at generality (that is, to not introduce any additional assumption or bias related to indoor localization), we model the localization error as a bivariate Gaussian distribution since it is the least informative[4] distribution for any given variance [37]. Specifically, we assume the localization error follows a bivariate Gaussian distribution with mean $\boldsymbol{\mu} = [0\ 0]^T$ and covariance matrix $\boldsymbol{\Sigma} = \sigma_e^2 \mathbf{I}_2$ as in [38]. Thus, x and y components of the localization error vector follow a Normal distribution:

$$x_{e,k}, y_{e,k} \sim \mathcal{N}\left(0, \sigma_e^2\right). \tag{18}$$

Moreover, the magnitude of the localization error vector follows a Rayleigh distribution:

$$f_R\left(r|\sigma_e^2\right) = \frac{r}{\sigma_e^2} \exp\left(-\frac{r^2}{2\sigma_e^2}\right), \quad r \geq 0, \tag{19}$$

where σ_e^2 is the scaling parameter. Finally, the angle of the localization error vector follows a uniform distribution:

$$\theta_{e,k} \sim \mathcal{U}(-\pi, \pi). \tag{20}$$

Let $r_{e,k}$, i.e., the radius of the localization error vector, represent the localization accuracy. Considering the bivariate Gaussian model, the localization accuracy follows the Rayleigh distribution. Thus, we have

$$\mathbb{E}\{r_{e,k}\} = \sigma_e\sqrt{\pi/2}, \tag{21}$$

$$\text{Var}\{r_{e,k}\} = \frac{4 - \pi}{2}\sigma_e^2. \tag{22}$$

In 3GPP standards, the localization accuracy requirements are typically specified in terms of the 95%-quantile [39]. The F-quantile of a Rayleigh distribution with scaling parameter σ_e is given by

$$Q(F; \sigma_e) = \sigma_e\sqrt{-2\ln(1 - F)}. \tag{23}$$

[4]In information theory and statistics, "least informative" refers to the distribution with the maximum entropy (i.e., uncertainty) for a given variance.

TABLE 2. Examples of localization accuracy requirements for pessimistic, optimistic, and reasonable scenarios [40], [41], [42].

σ_e^2	95% Quantile	Scenario
5 dB	4.5 m	Pessimistic
1.76 dB	3 m	Reasonable
−7.8 dB	1 m	Reasonable
−28 dB	10 cm	Optimistic
−45 dB	1 cm	Optimistic

Considering the proposed localization error model and based on the 3GPP specifications, we list examples of localization accuracy requirements for pessimistic, reasonable, and optimistic scenarios and their corresponding values of σ_e^2 in Table 2. In 3GPP Rel-16, the localization accuracy requirement specified for indoor scenarios was 3 m [40]. In 3GPP Rel-17, this requirement was further reduced to 20 cm [41]. The localization accuracy requirement for beyond-5G and 6G networks in indoor factory scenarios is expected to be in the order of a few centimeters [42].

IV. OPTIMAL ANGULAR POSITIONS OF THE RULAS

In each time slot, K distinct MTDs are active. Our previous work [18] shows a distinct optimal angular position for the RULA for each subset of K locations of active MTDs. Moreover, high-speed industrial servo motors can change their angular positions within a few milliseconds[5] with very high precision [43], [44]. Thus, they can track slow-to-moderate network dynamics in practice. Moreover, assuming the ULA is implemented as a microstrip patch antenna array, similar to the prototypes studied in [45], [46], [47], [48], it will be lightweight. Hence, it will not impose a significant payload burden on the servo motor.

Let $\theta_q \in [-\pi, \pi]$ denote the rotation of the RULA of the q-th AP. A RULA and its angular position concerning two

[5]In this work, we assume that the rotation of the RULAs is performed only once and before the uplink data transmission phase. Consequently, the time required to rotate the RULAs does not yield channel aging or any other impact on the uplink data transmission. Nevertheless, timing requirements are crucial for the operation of our proposed system, and we intend to study them more thoroughly in future extensions of this work.
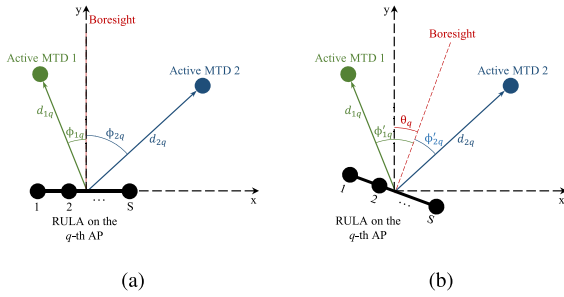
FIGURE 3. Illustration of the RULA of the *q*-th AP and its angular positions concerning two active MTDs (a) before the rotation and (b) after the rotation.

active MTDs, before and after its rotation, is illustrated in Fig. 3. The angle between the *k*-th MTD and the *q*-th AP after the rotation of the RULA is given by [8]

$$\phi'_{kq} := \phi_{kq} + \theta_q. \tag{24}$$

The optimal rotations of the RULAs $\theta_q; \forall q \in \{1, \ldots, Q\}$, are jointly computed by the CPU as a function of $\hat{\mathbf{p}}_k, \forall k \in \{1, \ldots, K\}$. This computation can be written as the following optimization problem:

$$\begin{aligned} \text{maximize } & f\big(\theta_1, \ldots, \theta_Q \mid \hat{\mathbf{p}}_k, \ k \in \{1, \ldots, K\}\big) \\ \text{subject to } & 0 \leq \theta_1, \ldots, \theta_Q \leq \pi, \end{aligned} \tag{25}$$

where $f(\cdot)$ is the objective function to be maximized. Owing to the large number of variables to be jointly optimized and the high non-linearity of this problem, it is solved using particle swarm optimization (PSO), which will be presented in the next subsection.

A. PARTICLE SWARM OPTIMIZATION

PSO [49, Ch. 16] is very suitable for solving problems where a function's global maximum or minimum is very difficult to find. The algorithm works over a population of candidate solutions, known as agents or particles, and moves them in the search space according to their current positions and velocities. Each particle's movement is influenced by its best-known position and the global best-known position in the search space. The local and global best positions are updated on each iteration, and the algorithm is expected to move the swarm of particles toward the optimal solution.

PSO was initially proposed in [50] and intended to simulate social behavior, such as the movement of organisms in a bird flock or fish school. It has been used to solve many optimization problems in communication systems, such as optimal deployment, node localization, clustering, and data aggregation in wireless sensor networks [51]. It has also been used to design antennas with a specific desired side-lobe level or antenna element positions in a non-uniform array [52]. In communication systems, it has also been used to compute the optimal precoding vector that maximizes the throughput of a multi-user MIMO system [53], to optimize the scheduling in the downlink of a multi-user MIMO system [54], and to initialize the channel estimates for MIMO-OFDM receivers that jointly perform channel estimation and decoding [55].

TABLE 3. Parameters of the PSO algorithm.

Symbol	Parameter
$f(\cdot)$	Objective function
x_i	Position of the i-th particle
v_i	Velocity of the i-th particle
w	Inertial weight
c_1	Cognitive constant
u_1, u_2	Random numbers between 0 and 1
c_2	Social constant
$p_{b,i}$	Personal best of the i-th particle
g_b	Global best

Algorithm 1 Particle Swarm Optimization

1: Initialize the swarm of particles uniformly distributed over the Q-th dimensional space $[0, \pi]^{Q \times 1}$
2: Initialize personal best positions as the current particle's positions: $p_{b,i}^0 \leftarrow x_i^0$
3: **while** the termination criterion is not met **do**
4:     **for** Each particle **do**
5:         Evaluate each particle's position considering the objective function
6:         **if** Current position is better than personal best **then**
7:             Update personal best position
8:         **end if**
9:         **if** Current position is better than global best **then**
10:            Update global best position
11:         **end if**
12:     **end for**
13:     **for** each particle **do**
14:         Update particles' velocities:
        $v_i^{t+1} \leftarrow wv_i^t + c_1 u_1^t (p_{b,i}^t - x_i^t) + c_2 u_2^t (g_b^t - x_i^t)$
15:         Move the particles to their next positions:
        $x_i^{t+1} \leftarrow x_i^t + v_i^t$
16:     **end for**
17: **end while**

The parameters of the PSO algorithm are listed in Table 5, while its pseudo-code is in Algorithm 1. The inertial weight w controls the particle's tendency to continue in its current direction, while c_1 and c_2 are the acceleration coefficients that control the influence of the personal and global best positions, respectively. In our optimization problem, the number of variables to be jointly optimized equals the number of APs, Q. Each particle is a candidate set of angular positions for the Q RULAs, i.e., $\{\theta_1, \ldots, \theta_Q\}$, which corresponds to a point in the Q-dimensional space with boundaries $[0, \pi]^{Q \times 1}$. The objective function depends on the estimates of the locations of the MTDs, i.e., $f(\hat{\mathbf{p}}_1, \ldots, \hat{\mathbf{p}}_K)$, and is described in the next Subsection. There are two possible termination criteria: i) the maximum number of iterations is reached, or ii) the relative change in the value of the global best over a predefined number of maximum stall iterations is less than the tolerance ϵ.
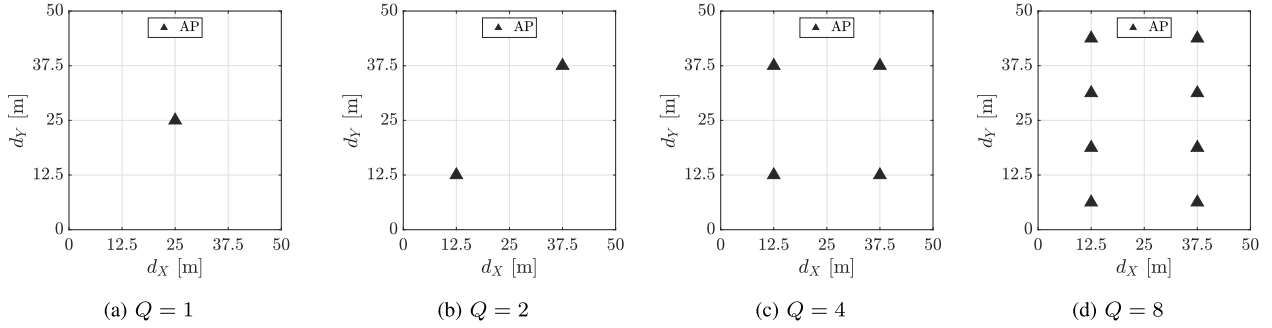
FIGURE 4. The square coverage area with $l = 50$ m and the four different setups of APs considered in this work.

PSO is suitable for the obtaining the maximum global or minimum of functions since its particles evaluate the function at multiple points at the same. Thus, the optimization problem is solved in a parallelized fashion, which significantly reduces the required computation time. Besides, having multiple particles distributed on the domain of the function makes it harder for the problem to converge to a local minimum or maximum point. Nevertheless, the major drawbacks of PSO are [56], [57], [58]:

1) There is no guarantee that it will indeed converge to the global minimum or maximum point because of its stochastic nature. The particles may become clustered around a local optimum point early in the optimization process, leading to premature convergence;

2) Depending on the problem, PSO may be very sensitive to the tuning of its parameters, such as the number of the particles, inertia weight, cognitive and social constants, and the maximum number of iterations;

3) PSO may present a very high computational cost when dealing with high-dimensions optimization problems (i.e., problems with many optimization variables) and not perform well at the same time.

B. LOCATION-BASED BEAMFORMING

Before *Phase 3* of the three-phase RA scheme, the CPU does not have any CSI information. Thus, the only information available for the computation of the optimal angular positions of the RULAs is the estimates of the locations of the MTDs that will be active in each time slot. Thus, we adopt a location-based beamforming [59], [60], [61], [62] approach to estimate the corresponding objective function value.

Herein, we assume that the locations of all the APs are perfectly known. Given $\hat{\mathbf{p}}_k$, $\forall k$, the CPU computes the estimates for the distances and azimuth angles between all the APs and the MTDs, i.e., $\hat{d}_{k,q}$ and $\hat{\phi}_{k,q}$, $\forall k$, $\forall q$. Then, it computes pseudo channel vectors assuming full-LoS propagation as

$$
\mathbf{h}_{kq}^{\text{pseudo}} = \sqrt{\hat{\beta}_{kq}}
\begin{bmatrix}
1 \\
\exp\!\left(-j2\pi \Delta \sin(\hat{\phi}_{kq})\right) \\
\exp\!\left(-j4\pi \Delta \sin(\hat{\phi}_{kq})\right) \\
\vdots \\
\exp\!\left(-j2\pi (S-1) \Delta \sin(\hat{\phi}_{kq})\right)
\end{bmatrix}, \quad (26)
$$

where $\hat{\beta}_{kq}$ is the estimated large-scale fading coefficient, which is computed as a function of the estimated distance $\hat{d}_{kq}$ considering a known channel model.

Then, receive combining vectors are computed as a function of the pseudo channel vectors according to (11). Finally, the cost function is obtained by computing the mean per-user achievable SE utilizing the pseudo-channel vectors and the corresponding receive combining vectors in (10), (12) and (13).

V. NUMERICAL RESULTS

In this section, we present Monte Carlo simulation results that evince the performance improvements obtained by APs equipped with the proposed RULAs when compared to APs equipped with static ULAs. We keep the total number of antenna elements constant and study the trade-off between the number of APs and antenna elements per AP. The square coverage area[6] with $l = 50$ m and the four different setups of APs considered for the simulations are illustrated in Fig. 4.

A. SIMULATION PARAMETERS

The power attenuation due to the distance (in dB) is modelled using the log-distance path loss model as

$$
\beta_{kq} = -L_0 - 10\eta \log_{10}\!\left(\frac{d_{kq}}{d_0}\right), \quad (27)
$$

where d_0 is the reference distance in meters, L_0 is the attenuation owing to the distance at the reference distance

---

[6]We opted to consider a square coverage area keeping in mind the shape of indoor industrial environments such as factory floors and warehouses. A square coverage area also facilitates the simulations, since it is simpler to uniformly distributed the APs this way. Moreover, we assuming circular or hexagonal areas should not lead to any relevant changes on the numerical results and conclusions. It should also be noted that in real-world scenarios, coverage areas can have irregular shapes.

TABLE 4. Simulation parameters.

Parameter	Symbol	Value
Total number of antenna elements	M	16
Number of APs	Q	$\{1, 2, 4, 8\}$
Number of antennas on each AP	S	$\{16, 8, 4, 2\}$
Number of active MTDs	K	10
Length of the side of the square area	l	$[50, 100, 200]$ m
Uplink transmission power	p	100 mW
PSD of the noise	N_0	4×10^{-21} W/Hz
Signal bandwidth	B	20 MHz
Noise figure	N_F	9 dB
Height of the APs	h_{AP}	12 m
Height of the UEs	h_{UE}	1.5 m
Carrier frequency	f_c	3.5 GHz
Normalized inter-antenna spacing	Δ	0.5
Path loss exponent	η	2
Reference distance	d_0	1 m

TABLE 5. Parameters of the PSO algorithm.

Symbol	Parameter	Value
w	Inertial weight	$[0.1, 1.1]$
c_1	Cognitive constant	1.49
c_2	Social constant	1.49
N_{vars}	Number of variables	Q
$|\mathcal{A}|$	Swarm size	$\min\{100, 10N_{vars}\}$
N_{max}	Maximum number of iterations	$200N_{vars}$
N_{stall}	Maximum number of stall iterations	20
ϵ	Function tolerance	10^{-6}

(in dB), η is the path loss exponent and d_{kq} is the distance between the k-th device and the q-th AP in meters.

The attenuation at the reference distance is calculated using the Friis free-space path loss model and given by

$$L_0 = 20 \log_{10}\left(\frac{4\pi d_0}{\lambda}\right), \tag{28}$$

where $\lambda = c/f_c$ is the wavelength in meters, c is the speed of light and f_c is the carrier frequency.

Unless stated otherwise, the values of the simulation parameters adopted in this work are listed in Table 4. Considering the typical values of M and h_{AP} defined in Table 4, every pair of AP and MTD are in the far-field (please refer to the Appendix). The active MTDs are uniformly distributed on the square coverage area, that is, $x_k, y_k \sim \mathcal{U}(0, l)$. Moreover, the adopted parameters for the PSO algorithm are listed in Table 5.

The noise power (in Watts) is given by $\sigma_n^2 = N_0 B N_F$, where N_0 is the Power Spectral Density (PSD) of the thermal noise in W/Hz, B is the signal bandwidth in Hz, and N_F is the noise figure at the receivers.

For the computation of the correlation matrices $\mathbf{R}_{kq}$, $\forall k$, $\forall q$, we consider $N = 6$ scattering clusters, $\psi_{kq,n} \sim \mathcal{U}[\phi_{kq} - 40°, \phi_{kq} + 40°]$, and $\sigma_\psi = 5°$.

B. SIMULATION RESULTS AND DISCUSSIONS

The mean per-user achievable SE is obtained by averaging over multiple network realizations, i.e., distinct sets of locations for the K active MTDs. For each network realization, the achievable SE of the K MTDs is obtained by averaging over several channel realizations, i.e., distinct realizations of the channel matrix $\mathbf{H}$.

The mean-per user achievable SE $\bar{R}$ as a function of the Rician factor κ, for different values of Q and l, are shown in Fig. 5. The primary motivation for obtaining $\bar{R}$ as a function of κ is to evaluate the performance of our proposed approach under a variety of different conditions. Different indoor industrial scenarios may feature diverse objects (varying in number, size and materials), the presence or absence of walls, leading to wireless channels that experience different Rician factors. We observe that, in the case of APs equipped with static ULAs, the mean per-user achievable SE decreases with the Rician factor for any values of Q and l. This happens because the correlation among the channel vectors increases with κ, thus affecting the performance obtained with the ZF combiner. On the other hand, in the case of APs equipped with the proposed RULAs, the mean per-user achievable SE increases with κ, excepted for the setups with $Q = 8$. This evinces the fact that the optimal rotation of the RULAs reduces the correlation between the channel vectors, consequently enhancing the performance obtained with ZF when the LoS component becomes strong. Note that, when $\kappa \leq -10$ dB, i.e., when the channel tends to be pure NLoS, the optimal rotation of the RULAs brings no performance improvements, as expected. Nevertheless, when κ grows large, the performance gains obtained with the RULAs become very significant for any values of Q and l. Moreover, when the channel tends to be pure NLoS, increasing Q enhances the mean per-user achievable SE for any value of l. Thus, in rich scattering environments, the most distributed D-MIMO setup with $Q = 8$ is always the best choice, and the setup with $Q = 4$ follows closely behind. In contrast, when κ grows large and the LoS component becomes strong, there exists an optimal number of APs (and of antenna elements per AP) that maximizes the mean per-user achievable SE.

The numerical results in Fig. 5 show that in the case of APs with static ULAs and under high Rician factor, the best performance is achieved by the setup with $Q = 2$ in the case of $l = 50$ m (Fig. 5a), and by the setups with $Q = 4$ for the cases of $l = 100$ m and $l = 200$ m (Figs. 5b and 5c, respectively). Conversely, when we adopt APs equipped with RULAs in the scenarios with high Rician factor, the single AP setup achieves the best performance for the case of $l = 50$ m (Fig. 5a). When $l = 100$ m (Fig. 5b), the setups with $Q = [1, 2, 4]$ achieve nearly identical performance. Finally, when $l = 200$ m (Fig. 5c), the best performance is achieved when $Q = 4$. Overall, the curves in Fig. 5 show that, when the LoS component is strong, there is a sweet spot between the beamforming gains obtained with APs equipped with multiple antennas, and the macro-diversity gains obtained
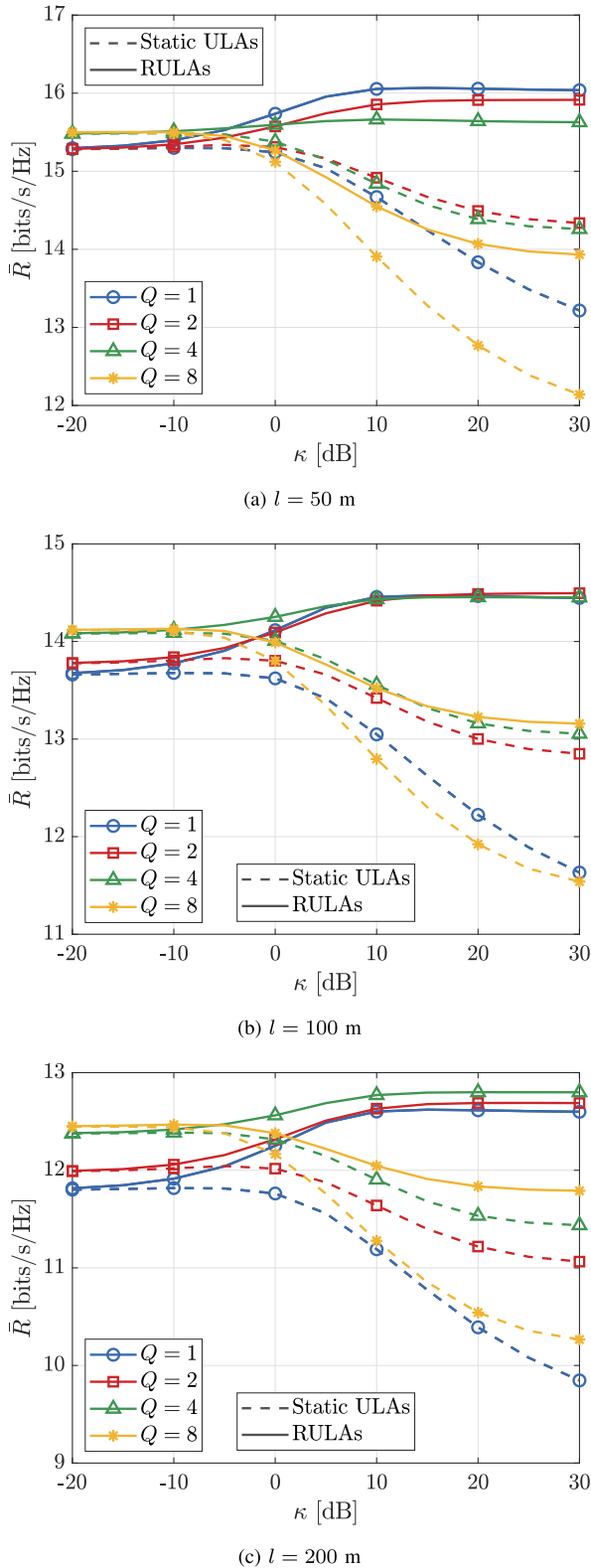
(a) $l = 50$ m

(b) $l = 100$ m

(c) $l = 200$ m

FIGURE 5. Mean per-user achievable SE versus Rician factor, considering centralized ZF and $\sigma_e^2 = -10$ dB, for different sizes of the square coverage area.

with the spatial distribution of APs. In the case of APs equipped with static ULAs, the intermediate deployments with $Q = [2, 4]$ achieve this sweet spot. Conversely, when the

proposed RULAs are adopted, utilizing a single AP allows us to achieve satisfactory performance while avoiding D-MIMO networks' higher deployment and maintenance costs.

In Fig. 6, we show the mean per-user achievable SE versus the variance of the localization error σ_e^2, for different values of Q and l, and considering $\kappa = 10$ dB. Note that all the curves in Fig. 6 corresponding to the case of static APs are constant since those setups do not use the estimated locations of the active MTDs for any optimization. As discussed in Section III, the scenarios where $\sigma_e^2 \geq 5$ dB, that is, with very poor location estimates, are not expected to occur in current or future wireless networks under normal operational conditions. We evaluate this range of variance of the localization error to illustrate the robustness of our proposed framework. Interestingly, we observe that the performance gains owing to the optimal rotations of the RULAs are still very significant even when the accuracy of the location estimates is poor. Nevertheless, the SE is almost constant for $\sigma_e^2 \leq -10$ dB, that is, improving the accuracy of the location estimates does not yield noticeable performance improvements. The curves in Fig. 6a show that, in the case of a small coverage area (specifically, $l = 50$ m), it is more advantageous to deploy fewer APs equipped with more antennas since the best performance is achieved with $Q = 2$ in the case of static ULAs and with $Q = 1$ in the case of the proposed RULAs. When we increase the size of the coverage area to $l = 100$ m and $l = 200$ m (Figs. 6b and 6c, respectively), we observe that the setup with $Q = 4$ achieves the best performance for both cases of static ULAs and RULAs. In the case of $l = 100$ m, the performance achieved with $Q = 1$ and $Q = 2$ when RULAs are adopted approach the performance obtained with $Q = 4$. These numerical results show that, as we increase the size of the coverage area, and given a total number of antenna elements M, a sweet spot between the number of APs and the number of antenna elements per AP becomes evident. This sweet spot corresponds to a trade-off between macro-diversity and beamforming gains. Finally, it is also very interesting to observe that in all the cases ($l = \{50, 100, 200\}$ m), the most distributed setup with $Q = 8$ presents the worst performance.

C. COMPLEXITY ANALYSIS OF PSO
The simulations ran on a personal computer having Windows 10, Intel Core i5-10210U processor and 32 GB of RAM memory. Besides, we utilized MATLAB version R2022b. The PSO was implemented on MATLAB using the `particleswarm` built-in function [63]. Since we utilized a built-in function of MATLAB, it is very difficult to measure the complexity of the PSO in terms of metrics such as number of float-point operations (FLOPs). Thus, we decided to analyse the computational complexity of our PSO solution in terms of the mean and the variance of the required time for the optimization algorithm to finish. This time can be measured in MATLAB using the functions `tic;toc` or `cputime`.
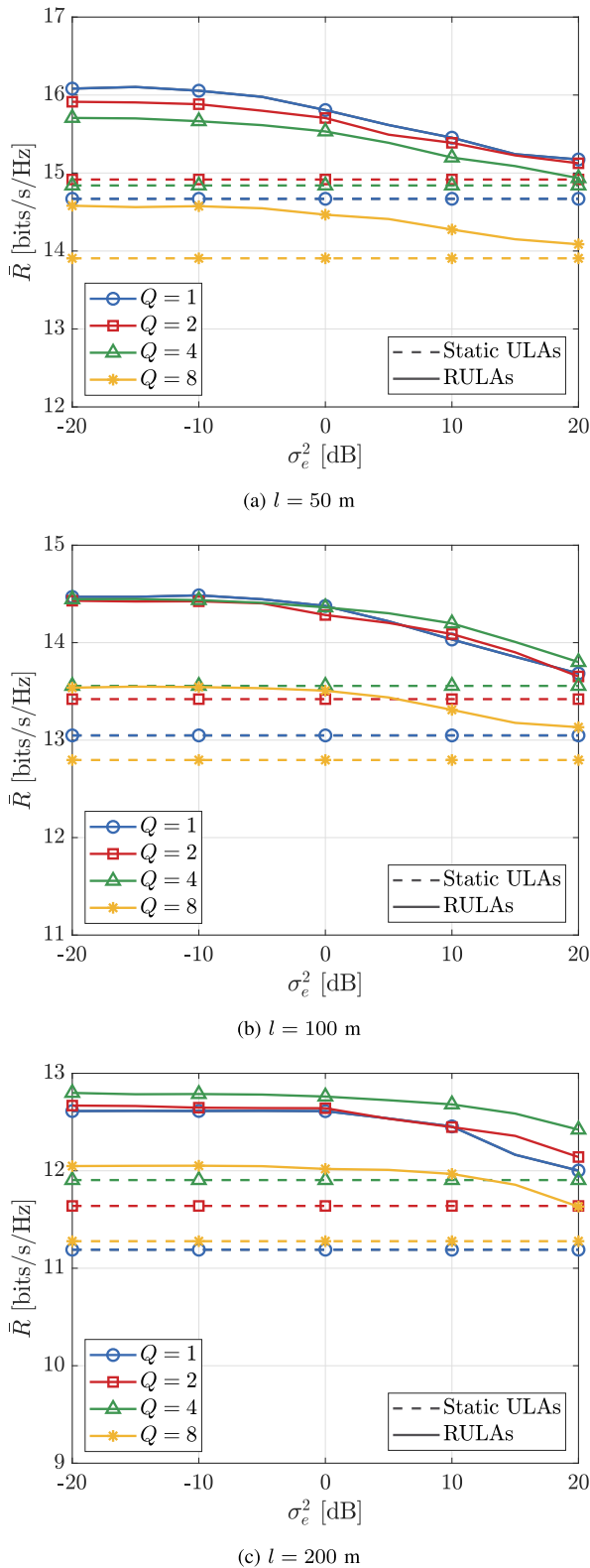
(a) $l = 50$ m

(b) $l = 100$ m

(c) $l = 200$ m

FIGURE 6. Mean per-user achievable SE versus the variance of the localization error, considering centralized ZF and $\kappa = 10$ dB, for different sizes of the square coverage area.

The mean and variance of the execution time can be found in Table 6. The PSO converges when the relative change in the value of the objective function over a

TABLE 6. Mean and variance of the execution time required for PSO to finish, considering $\kappa = 10$ dB, $\sigma_e^2 = -10$ dB and $l = 100$ m.

Number of RULAs	$Q = 1$	$Q = 2$	$Q = 4$	$Q = 8$
Mean	0.2652 s	0.6042 s	2.1520 s	7.9548 s
Variance	0.0363 s^2	0.0636 s^2	0.4624 s^2	7.3269 s^2

given number of "maximum stall iterations" is less than the "function tolerance" [63]. We observe that the mean required time increases rapidly with the number of RULAs Q (i.e., the number of optimization variables). Therefore, PSO indeed may not be the best choice in D-MIMO networks with multiple RULAs whose angular positions are jointly optimized by the CPU. Moreover, the mean required time for any given value of Q indicates that it is impractical to optimize the angular positions of the RULAs at every time slot. In other words, the angular positions should not be adjusted too often. In the framework we propose, the RULAs' angular positions are adjusted a single time, prior to the uplink data transmission phase. Subsequently, the angular positions remain unchanged throughout multiple time slots during the uplink data transmission phase.

VI. CONCLUSION

In this work, we studied the performance of D-MIMO networks for indoor scenarios. Aiming to enhance the quality of the wireless links, we proposed the deployment of APs equipped with RULAs. The CPU jointly computes the optimal rotation of the RULAs as a function of the estimated locations of the active MTDs. The optimization is done using a location-based beamforming approach and PSO. We considered a spatially correlated Rician fading model and evaluated the setups' performance for different Rician factor values. We took into account the impact of imperfect localization information and also of the imperfect CSI. Given the total number of antenna elements, we evaluated the trade-off between the number of APs and antennas per AP. The numerical results show that the optimal rotation of the RULAs can bring substantial performance gains in terms of mean per-user achievable SE, and the gains grow with the Rician factor. We also observed that the optimal rotation of the RULAs can bring performance gains even when the localization accuracy is poor or moderate. We also concluded that, given the total number of antenna elements, there is a sweet spot between the number of APs and the number of antenna elements per AP, corresponding to a trade-off between beamforming and macro-diversity gains. The best performance is achieved by adopting a few APs equipped with multiple antennas. This approach also has the advantage of reducing the deployment and maintenance costs of the system and its computational complexity.

This work studied the performance gains in terms of SE that the rotation of the ULAs can bring to wireless communications. Nevertheless, Integrated Sensing and

Communications (ISAC) is a research topic that has become extremely popular in both academia and industry. Some recent works [64], [65], [66] have evaluated the performance improvements in the accuracy of sensing and localization obtained with the movement of antennas. The movement of antennas can be beneficial in several ways. For instance, it can help overcome blockages in the line-of-sight between an access point (AP) and a device. Additionally, by allowing for precise beamforming and optimal beamwidth design, movable antennas can enhance data transmission and improve sensing accuracy. This capability reduces undesirable side lobes and improves interference management. Furthermore, movable antennas can dynamically switch between optimal array geometries, depending on whether they are used for sensing or communication applications. Comparing different implementations of movable and/or rotary antennas and the associated performance improvements for both sensing and communications is a promising direction for future works.

APPENDIX
PARAMETERS TO ENSURE FAR-FIELD PROPAGATION

The Fraunhofer distance determines the threshold between the near-field and far-field propagation and is given by [67]

$$d_F = \frac{2D^2}{\lambda}, \tag{29}$$

where D is the largest dimension of the antenna array, $\lambda = c/f_c$ is the wavelength, c is the speed of the light and f_c is the carrier frequency. In the case of an RULA with half-wavelength spaced antenna elements, we have

$$D_{\text{RULA}} = (S-1)\lambda/2, \tag{30}$$

where S is the number of antenna elements of the RULA. Considering $f_c = 3.5$ GHz, the height difference between the APs and the MTDs must be at least 10 m to ensure far-field propagation conditions for all the devices. Thus, in this paper we set $\max\{S\} = M = 16$ and $h_{\text{AP}} = 12$ m.

REFERENCES

[1] H. Shariatmadari et al., "Machine-type communications: Current status and future perspectives toward 5G systems," *IEEE Commun. Mag.*, vol. 53, no. 9, pp. 10–17, Sep. 2015.

[2] M. Wen et al., "Private 5G networks: Concepts, architectures, and research landscape," *IEEE J. Sel. Topics Signal Process.*, vol. 16, no. 1, pp. 7–25, Jan. 2022.

[3] M. A. Uusitalo et al., "6G vision, value, use cases and technologies from European 6G flagship project Hexa-X," *IEEE Access*, vol. 9, pp. 160004–160020, 2021.

[4] H. Q. Ngo, A. Ashikhmin, H. Yang, E. G. Larsson, and T. L. Marzetta, "Cell-free massive MIMO versus small cells," *IEEE Trans. Wireless Commun.*, vol. 16, no. 3, pp. 1834–1850, Mar. 2017.

[5] Z. Chen and E. Björnson, "Channel hardening and favorable propagation in cell-free massive MIMO with stochastic geometry," *IEEE Trans. Commun.*, vol. 66, no. 11, pp. 5205–5219, Nov. 2018.

[6] G. Interdonato, E. Björnson, H. Q. Ngo, P. Frenger, and E. G. Larsson, "Ubiquitous cell-free massive MIMO communications," *EURASIP J. Wireless Commun. Netw.*, vol. 2019, no. 1, p. 197, 2019.

[7] H. Do, N. Lee, and A. Lozano, "Reconfigurable ULAs for line-of-sight MIMO transmission," *IEEE Trans. Wireless Commun.*, vol. 20, no. 5, pp. 2933–2947, May 2021.

[8] O. L. A. López, F. A. Monteiro, H. Alves, R. Zhang, and M. Latva-Aho, "A low-complexity beamforming design for multiuser wireless energy transfer," *IEEE Wireless Commun. Lett.*, vol. 10, no. 1, pp. 58–62, Jan. 2021.

[9] O. L. A. López, F. A. Monteiro, H. Alves, R. Zhang, and M. Latva-Aho, "CSI-free rotary antenna beamforming for massive RF wireless energy transfer," *IEEE Internet Things J.*, vol. 9, no. 10, pp. 7375–7387, May 2022.

[10] K. Lin, O. L. A. López, H. Alves, and T. Hao, "On CSI-free multiantenna schemes for massive wireless-powered underground sensor networks," *IEEE Internet Things J.*, vol. 10, no. 19, pp. 17557–17570, Oct. 2023.

[11] A. Zubow, A. Memedi, and F. Dressler, "Towards hybrid electronic-mechanical beamforming for IEEE 802.11ad," in *Proc. 18th Wireless Demand Netw. Syst. Serv. Conf. (WONS)*, 2023, pp. 88–91.

[12] L. Zhu, W. Ma, and R. Zhang, "Movable antennas for wireless communication: Opportunities and challenges," *IEEE Commun. Mag.*, vol. 62, no. 6, pp. 114–120, Jun. 2024.

[13] Z. Xiao, X. Pi, L. Zhu, X.-G. Xia, and R. Zhang, "Multiuser communications with movable-antenna base station: Joint antenna positioning, receive combining, and power control," 2023, *arXiv:2308.09512*.

[14] L. Zhu, W. Ma, and R. Zhang, "Modeling and performance analysis for movable antenna enabled wireless communications," *IEEE Trans. Wireless Commun.*, vol. 23, no. 6, pp. 6234–6250, Jun. 2024.

[15] J. Li, Z. Lin, S. G. Razul, A. A. Kumar, Y. Zheng, and C.-M. See, "DOA estimation with a rotational uniform linear array (RULA) and unknown spatial noise covariance," *Multidimensional Syst. Signal Process.*, vol. 29, pp. 537–561, Apr. 2018.

[16] G. Amponis et al., "Drones in B5G/6G networks as flying base stations," *Drones*, vol. 6, no. 2, p. 39, 2022.

[17] S. A. H. Mohsan, N. Q. H. Othman, Y. Li, M. H. Alsharif, and M. A. Khan, "Unmanned Aerial Vehicles (UAVs): Practical aspects, applications, open challenges, security issues, and future trends," *Intell. Serv. Robot.*, vol. 16, no. 1, pp. 109–137, 2023.

[18] E. N. Tominaga, O. L. A. López, T. Svensson, R. D. Souza, and H. Alves, "On the spectral efficiency of indoor wireless networks with a rotary uniform linear array," 2024, *arXiv:2402.05583*.

[19] E. Nayebi, A. Ashikhmin, T. L. Marzetta, H. Yang, and B. D. Rao, "Precoding and power optimization in cell-free massive MIMO systems," *IEEE Trans. Wireless Commun.*, vol. 16, no. 7, pp. 4445–4459, Jul. 2017.

[20] G. Femenias, F. Riera-Palou, A. Álvarez-Polegre, and A. García-Armada, "Short-term power constrained cell-free massive-MIMO over spatially correlated Ricean fading," *IEEE Trans. Veh. Technol.*, vol. 69, no. 12, pp. 15200–15215, Dec. 2020.

[21] S. Chen, J. Zhang, E. Björnson, J. Zhang, and B. Ai, "Structured massive access for scalable cell-free massive MIMO systems," *IEEE J. Sel. Areas Commun.*, vol. 39, no. 4, pp. 1086–1100, Apr. 2021.

[22] Ö. Özdogan, E. Björnson, and E. G. Larsson, "Massive MIMO with spatially correlated Rician fading channels," *IEEE Trans. Commun.*, vol. 67, no. 5, pp. 3234–3250, May 2019.

[23] D. Kumar, O. L. A. López, A. Tölli, and S. Joshi, "Latency-aware joint transmit beamforming and receive power splitting for SWIPT systems," in *Proc. IEEE 32nd Annu. Int. Symp. Pers. Indoor Mobile Radio Commun. (PIMRC)*, 2021, pp. 490–494.

[24] E. Björnson, J. Hoydis, and L. Sanguinetti, "Massive MIMO networks: Spectral, energy, and hardware efficiency," *Found. Trends® Signal Process.*, vol. 11, no. 3-4, pp. 154–655, 2017.

[25] M. Alonzo, P. Baracca, S. R. Khosravirad, and S. Buzzi, "Cell-free and user-centric massive MIMO architectures for reliable communications in indoor factory environments," *IEEE Open J. Commun. Soc.*, vol. 2, pp. 1390–1404, 2021.

[26] A. Paulraj, R. Nabar, and D. Gore, *Introduction to Space-Time Wireless Communications*. Cambridge, U.K.: Cambridge Univ. Press, 2003.

[27] P. Liu et al., "Spectral efficiency analysis of cell-free massive MIMO systems with zero-forcing detector," *IEEE Trans. Wireless Commun.*, vol. 19, no. 2, pp. 795–807, Feb. 2020.

[28] O. L. A. López, D. Kumar, R. D. Souza, P. Popovski, A. Tölli, and M. Latva-Aho, "Massive MIMO with radio stripes for indoor wireless energy transfer," *IEEE Trans. Wireless Commun.*, vol. 21, no. 9, pp. 7088–7104, Sep. 2022.

[29] C. Wang, T. C.-K. Liu, and X. Dong, "Impact of channel estimation error on the performance of amplify-and-forward two-way relaying," *IEEE Trans. Veh. Technol.*, vol. 61, no. 3, pp. 1197–1207, Mar. 2012.

[30] E. Eraslan, B. Daneshrad, and C.-Y. Lou, "Performance indicator for MIMO MMSE receivers in the presence of channel estimation error," *IEEE Wireless Commun. Letters*, vol. 2, no. 2, pp. 211–214, Apr. 2013.

[31] Z. Dawy, W. Saad, A. Ghosh, J. G. Andrews, and E. Yaacoub, "Toward massive machine type cellular communications," *IEEE Wireless Commun.*, vol. 24, no. 1, pp. 120–128, Feb. 2017.

[32] P. H. J. Nardelli, M. de Castro Tomé, H. Alves, C. H. M. de Lima, and M. Latva-aho, "Maximizing the link throughput between smart meters and aggregators as secondary users under power and outage constraints," *Ad Hoc Netw.*, vol. 41, pp. 57–68, May 2016.

[33] J. Kang and W. Yu, "Scheduling versus contention for massive random access in massive MIMO systems," *IEEE Trans. Commun.*, vol. 70, no. 9, pp. 5811–5824, Sep. 2022.

[34] H. Liu, H. Darabi, P. Banerjee, and J. Liu, "Survey of wireless indoor positioning techniques and systems," *IEEE Trans. Syst. Man Cybern. Part-C (Appl. Rev.)*, vol. 37, no. 6, pp. 1067–1080, Nov. 2007.

[35] A. Yassin et al., "Recent advances in indoor localization: A survey on theoretical approaches and applications," *IEEE Commun. Surveys Tuts.*, vol. 19, no. 2, pp. 1327–1346, 2nd Quart., 2017.

[36] F. Zafari, A. Gkelias, and K. K. Leung, "A survey of indoor localization systems and technologies," *IEEE Commun. Surveys Tuts.*, vol. 21, no. 3, pp. 2568–2599, 3rd Quart., 2019.

[37] F. Gustafsson and F. Gunnarsson, "Mobile positioning using wireless networks: Possibilities and fundamental limitations based on available wireless network measurements," *IEEE Signal Process. Mag.*, vol. 22, no. 4, pp. 41–53, Jul. 2005.

[38] B. Zhu, Z. Zhang, and J. Cheng, "Outage analysis and beamwidth optimization for positioning-assisted beamforming," *IEEE Commun. Lett.*, vol. 26, no. 7, pp. 1543–1547, Jul. 2022.

[39] "Service requirements for the 5G system; (Release 15), Version 15.9.0," 3GPP, Sophia Antipolis, France, Rep. TS 22.261, 2019.

[40] "Study on NR positioning support; (Release 16), Version 16.0.0," 3GPP, Sophia Antipolis, France, Rep. TS 38.855, Mar. 2019.

[41] "Study on NR positioning support; (Release 17)," 3GPP, Sophia Antipolis, France, Rep. TS 38.857, Mar. 2021.

[42] J. Nikonowicz, A. Mahmood, M. I. Ashraf, E. Björnson, and M. Gidlund, "Indoor positioning in 5G-advanced: Challenges and solution toward centimeter-level accuracy with carrier phase enhancements," *IEEE Wireless Commun.*, vol. 31, no. 4, pp. 268–275, Aug. 2024.

[43] "Precision servo motor." Constar. 2023. [Online]. Available: http://constarmotor.com/productlist/2168.html#E_2189

[44] "Sigma-5 servo products." Yaskawa. 2023. [Online]. Available: https://www.yaskawa.com/products/motion/sigma-5-servo-products

[45] N. K. Host, C.-C. Chen, J. L. Volakis, and F. A. Miranda, "Low cost beam-steering approach for a series-fed array," in *Proc. IEEE Int. Symp. Phased Array Syst. Technol.*, 2013, pp. 293–300.

[46] V. K. Kothapudi, "SFCFOS uniform and Chebyshev amplitude distribution linear array antenna for K-band applications," *J. Electromagn. Eng. Sci.*, vol. 19, no. 1, pp. 64–70, 2019.

[47] B. Liu, A. P. Guevara, S. D. Bast, Q. Wang, and S. Pollin, "Massive MIMO indoor localization with 64-antenna uniform linear array," in *Proc. IEEE 91st Veh. Technol. Conf. (VTC)*, 2020, pp. 1–5.

[48] T. Iye, K. Tsuda, and Y. Fujii, "An experimental study of 28 GHz analog beamforming with a uniform linear array," in *Proc. 23rd Int. Conf. Adv. Commun. Technol. (ICACT)*, 2021, pp. 100–103.

[49] A. P. Engelbrecht, *Computational Intelligence: An Introduction*. Hoboken, NJ, USA: Wiley, 2007.

[50] J. Kennedy and R. Eberhart, "Particle swarm optimization," in *Proc. Int. Conf. Neural Netw. (ICNN)*, 1995, pp. 1942–1948.

[51] R. V. Kulkarni and G. K. Venayagamoorthy, "Particle swarm optimization in wireless-sensor networks: A brief survey," *IEEE Trans. Syst. Man Cybern. Part-C (Appl. Rev.)*, vol. 41, no. 2, pp. 262–267, Mar. 2011.

[52] N. Jin and Y. Rahmat-Samii, "Advances in particle swarm optimization for antenna designs: Real-number, binary, single-objective and multiobjective implementations," *IEEE Trans. Antennas Propag.*, vol. 55, no. 3, pp. 556–567, Mar. 2007.

[53] F. Shu, W. Gang, and L. Shao-Qian, "Optimal multiuser MIMO linear precoding with LMMSE receiver," *EURASIP J. Wireless Commun. Netw.*, vol. 2009, Aug. 2009, Art. no. 197682.

[54] Y. Hei, X. Li, K. Yi, and H. Yang, "Novel scheduling strategy for downlink multiuser MIMO system: Particle swarm optimization," *Sci. China Ser. F, Inf. Sci.*, vol. 52, no. 12, pp. 2279–2289, 2009.

[55] C. Knievel, P. A. Hoeher, A. Tyrrell, and G. Auer, "Particle swarm enhanced graph-based channel estimation for MIMO-OFDM," in *Proc. IEEE 73rd Veh. Technol. Conf. (VTC)*, 2011, pp. 1–5.

[56] K. E. Parsopoulos and M. N. Vrahatis, "Recent approaches to global optimization problems through particle swarm optimization," *Nat. Comput.*, vol. 1, pp. 235–306, Jun. 2002.

[57] D. Sedighizadeh and E. Masehian, "Particle swarm optimization methods, taxonomy and applications," *Int. J. Comput. Theory Eng.*, vol. 1, no. 5, pp. 486–502, 2009.

[58] T. M. Shami, A. A. El-Saleh, M. Alswaitti, Q. Al-Tashi, M. A. Summakieh, and S. Mirjalili, "Particle swarm optimization: A comprehensive survey," *IEEE Access*, vol. 10, pp. 10031–10061, 2022.

[59] R. Maiberger, D. Ezri, and M. Erlihson, "Location based beamforming," in *Proc. IEEE 26th Conv. Elect. Electron. Eng. Israel*, 2010, pp. 184–187.

[60] P. Kela et al., "Location based beamforming in 5G ultra-dense networks," in *Proc. IEEE 84th Veh. Technol. Conf. (VTC)*, 2016, pp. 1–7.

[61] S. Yan and R. Malaney, "Location-based beamforming for enhancing secrecy in Rician wiretap channels," *IEEE Trans. Wireless Commun.*, vol. 15, no. 4, pp. 2780–2791, Apr. 2016.

[62] C. Liu and R. Malaney, "Location-based beamforming and physical layer security in Rician wiretap channels," *IEEE Trans. Wireless Commun.*, vol. 15, no. 11, pp. 7847–7857, Nov. 2016.

[63] "Particle swarm optimization." MathWorks. 2024. Accessed: Aug. 22, 2024. [Online]. Available: https://se.mathworks.com/help/gads/particleswarm.html

[64] W. Ma, L. Zhu, and R. Zhang, "Movable antenna enhanced wireless sensing via antenna position optimization," 2024, *arXiv:2405.01215*.

[65] W. Lyu, S. Yang, Y. Xiu, Z. Zhang, C. Assi, and C. Yuen, "Flexible beamforming for movable antenna-enabled integrated sensing and communication," 2024, *arXiv:2405.10507*.

[66] A. Khalili and R. Schober, "Advanced ISAC design: Movable antennas and accounting for dynamic RCS," 2024, *arXiv:2407.20930*.

[67] J. Sherman, "Properties of focused apertures in the fresnel region," *IRE Trans. Antennas Propag.*, vol. 10, no. 4, pp. 399–408, Jul. 1962.

EDUARDO N. TOMINAGA (Graduate Student Member, IEEE) was born in São Paulo, Brazil, in 1995. He received the B.Sc. degree in electronics engineering from the Federal University of Santa Catarina, Florianópolis, Brazil, in 2019, and the M.Sc. degree in wireless communications engineering from the University of Oulu, Finland, in 2021, where he is currently pursuing the D.Sc. degree in communications engineering with the Centre for Wireless Communications. In 2023, he visited Nokia Bell Labs, Murray Hill, NJ, USA, and the Communication Systems Group, Chalmers University of Technology, Gothenburg, Sweden. His main research interests include wireless communications and digital signal processing.

ONEL L. A. LÓPEZ (Senior Member, IEEE) was born in Sancti-Spíritus, Cuba, in 1989. He received the B.Sc. degree (Hons.) in electrical engineering from the Central University of Las Villas, Cuba, in 2013, the M.Sc. degree in electrical engineering from the Federal University of Paraná, Brazil, in 2017, and the D.Sc. degree (Hons.) in electrical engineering from the University of Oulu, Finland, in 2020. From 2013 to 2015, he was a Specialist in telematics with Cuban telecommunications company (ETECSA). He currently holds an Assistant Professorship (tenure track) of Sustainable Wireless Communications Engineering with the Centre for Wireless Communications, University of Oulu. He is the co-author of the books titled *Wireless RF Energy Transfer in the Massive IoT Era: Towards Sustainable Zero Energy Networks* (Wiley, 2021) and *Ultra Reliable Low-Latency Communications: Foundations, Enablers, System Design, and Evolution Towards 6G* (Now Publishers, 2023). His research interests include sustainable IoT, energy harvesting, wireless RF energy transfer, wireless connectivity, machine-type communications, and cellular-enabled positioning systems. He was a recipient of the 2020 Best Doctoral Thesis Award granted by Academic Engineers and Architects in Finland TEK and Tekniska Föreningen i Finland in 2021 and the 2022 Young Researcher Award in the field of technology in Finland. He was a corecipient of the 2019 and 2023 IEEE European Conference on Networks and Communications Best Student Paper Award. He is a Collaborator to the 2016 Research Award given by the Cuban Academy of Sciences.

RICHARD D. SOUZA (Senior Member, IEEE) received the D.Sc. degree in electrical engineering from the Federal University of Santa Catarina (UFSC), Florianópolis, Brazil, in 2003. From 2004 to 2016, he was with the Federal University of Technology-Paraná, Curitiba, Brazil. Since 2017, he has been with UFSC, where he is a Professor with the Department of Electrical and Electronics Engineering. His research interests are in the areas of wireless communications and signal processing. He is the Supervisor of the Awarded Best Ph.D. Thesis in Electrical Engineering in Brazil in 2014, and a co-recipient of the 2016 Research Award from the Cuban Academy of Sciences. He has served as an Editor or an Associate Editor for the *Journal of Communication and Information Systems* (SBrT), the IEEE COMMUNICATIONS LETTERS, the IEEE TRANSACTIONS ON VEHICULAR TECHNOLOGY, the IEEE TRANSACTIONS ON COMMUNICATIONS, and the IEEE INTERNET OF THINGS JOURNAL.

TOMMY SVENSSON (Senior Member, IEEE) received the Ph.D. degree in information theory from Chalmers University of Technology, Gothenburg, Sweden, in 2003, where he is currently a Full Professor of Communication Systems and is also leading the wireless systems research on air interface and wireless backhaul networking technologies for future wireless systems. He was the Coordinator of the Communication Engineering Master's Program, Chalmers University of Technology. He was with Ericsson AB in core networks, radio access networks, and microwave transmission products. He was involved in the European WINNER and ARTIST4G Projects, which made important contributions to the 3GPP LTE Standards, the EU FP7 METIS, and the EU H2020 5GPPP mmMAGIC and 5GCar projects toward 5G, recently the Hexa-X, RISE-6G, and SEMANTIC Projects and the Hexa-X-II, ROBUST-6G, and ECO-eNET projects toward 6G. He is also active with the WiTECH Antenna Systems Excellence Center, Chalmers University of Technology targeting cm/mm-wave and (sub)-THz solutions for 6G access, backhaul/fronthaul, and V2X scenarios. He has co-authored six books. His research interests include mobile communication systems, cooperative/context-aided/secure communications, mm-wave/sub-THz communications, C-V2X, JCAS, satellite networks, and sustainability.

HIRLEY ALVES (Member, IEEE) received the B.Sc. and M.Sc. degrees in electrical engineering from the Federal University of Technology-Paraná (UTFPR), Curitiba, Brazil, in 2010 and 2011, respectively, and the dual D.Sc. degree from the University of Oulu, Oulu, Finland, and UTFPR in 2015. He is an Associate Professor and the Head of the Machine-Type Wireless Communications Group, 6G Flagship Centre for Wireless Communications, University of Oulu. He is actively working on massive connectivity and ultrareliable low-latency communications for future wireless networks, 5G and 6G, full-duplex communications, and physical-layer security. He leads the MTC activities for the 6G Flagship Program. He has received several awards and has been the organizer, the chair, the TPC, and the tutorial lecturer for several renowned international conferences. He is the General Chair of the ISWCS'2019 and the General Co-Chair of the 1st 6G Wireless Summit, Levi 2019, and ISWCS 2021.